

AD-A165 279

THE SPECIFICATION OF LATERAL BOUNDARY CONDITIONS IN  
THREE-DIMENSIONAL MES (U) LOWELL UNIV MA DEPT OF EARTH  
SCIENCE K L SEITTER 01 OCT 85 SCIENTIFIC-1

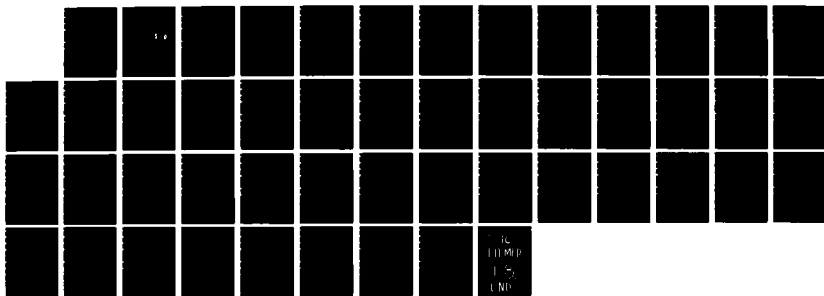
1/1

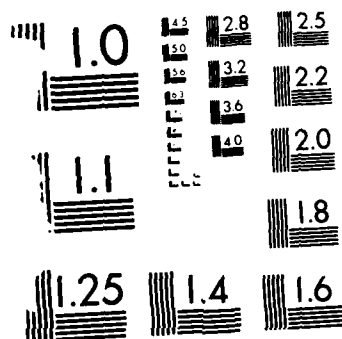
UNCLASSIFIED

AFGL-TR-86-0005 F19628-85-K-0008

F/G 8/3

NL





MICROCOPY RESOLUTION TEST CHART  
NATIONAL BUREAU OF STANDARDS-1963-A

# AD-A165 279

12

AFGL-TR-86-0005

THE SPECIFICATION OF LATERAL BOUNDARY CONDITIONS  
IN THREE-DIMENSIONAL MESOSCALE NUMERICAL MODELS

Keith L. Seitter

University of Lowell  
Department of Earth Sciences  
Lowell, MA

1 October 1985

Scientific Report No. 1

DTIC  
ELECTE  
MAR 17 1986  
S D

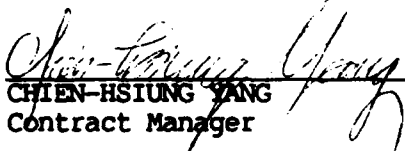
APPROVED FOR PUBLIC RELEASE; DISTRIBUTION UNLIMITED

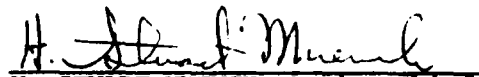
AIR FORCE GEOPHYSICS LABORATORY  
AIR FORCE SYSTEMS COMMAND  
UNITED STATES AIR FORCE  
HANSOM AIR FORCE BASE, MASSACHUSETTS 01731

DTIC FILE COPY


86 3 17 156

This technical report has been reviewed and is approved for publication.

  
CHIENT-HSIUNG YANG  
Contract Manager

  
H. STUART MUENCH, Acting Chief  
Atmospheric Prediction Branch

FOR THE COMMANDER

  
DONALD D. GRANTHAM, Acting Director  
Atmospheric Sciences Division

This report has been reviewed by the ESD Public Affairs Office (PA) and is releasable to the National Technical Information Service (NTIS).

Qualified requestors may obtain additional copies from the Defense Technical Information Center. All others should apply to the National Technical Information Service.

If your address has changed, or if you wish to be removed from the mailing list, or if the addressee is no longer employed by your organization, please notify AFGL/DAA, Hanscom AFB, MA 01731. This will assist us in maintaining a current mailing list.

Do not return copies of this report unless contractual obligations or notices on a specific document require that it be returned.

Unclassified

SECURITY CLASSIFICATION OF THIS PAGE

## REPORT DOCUMENTATION PAGE

1a. REPORT SECURITY CLASSIFICATION <b>Unclassified</b>			1b. RESTRICTIVE MARKINGS	
2a. SECURITY CLASSIFICATION AUTHORITY			3. DISTRIBUTION/AVAILABILITY OF REPORT  Approved for public release; Distribution unlimited.	
2b. DECLASSIFICATION/DOWNGRADING SCHEDULE			5. MONITORING ORGANIZATION REPORT NUMBER(S)  AFGL-TR-86-0005	
4. PERFORMING ORGANIZATION REPORT NUMBER(S)			7a. NAME OF MONITORING ORGANIZATION  Air Force Geophysics Laboratory	
6a. NAME OF PERFORMING ORGANIZATION  University of Lowell		6b. OFFICE SYMBOL (If applicable)	7b. ADDRESS (City, State and ZIP Code)  Hanscom AFB Massachusetts 01731	
6c. ADDRESS (City, State and ZIP Code)  Department of Earth Sciences Lowell, MA			8a. NAME OF FUNDING/SPONSORING ORGANIZATION	
8b. OFFICE SYMBOL (If applicable)			9. PROCUREMENT INSTRUMENT IDENTIFICATION NUMBER  F19628-85-K-0008	
8c. ADDRESS (City, State and ZIP Code)			10. SOURCE OF FUNDING NOS.	
			PROGRAM ELEMENT NO.  61102F	PROJECT NO.  2310
			TASK NO.  G7	WORK UNIT NO.  AH
11. TITLE (Include Security Classification) The Specification of Lateral Boundary Conditions in Three-Dimensional Mesoscale Numerical Models				
12. PERSONAL AUTHOR(S) Keith L. Seitter				
13a. TYPE OF REPORT  Scientific #1		13b. TIME COVERED FROM _____ TO _____		14. DATE OF REPORT (Yr., Mo., Day)  1985 October 1
15. PAGE COUNT				
16. SUPPLEMENTARY NOTATION				
17. COSATI CODES			18. SUBJECT TERMS (Continue on reverse if necessary and identify by block number)	
FIELD	GROUP	SUB GR.	Lateral boundary conditions	
			sponge conditions	
			radiation conditions	
			shallow water model	
19. ABSTRACT (Continue on reverse if necessary and identify by block number) A difficult aspect of numerical modeling on the meso-beta scale is the specification of values on the lateral boundaries. This study uses a one-dimensional shallow water model with parameters appropriately specified for this scale to investigate a number of lateral boundary condition formulations. Two geostrophically imbalanced initial conditions are used to test the boundary condition formulations. The scale of the disturbances was much smaller than the Rossby radius of deformation and the adjustment process was completed rapidly by the redistribution of the height field by waves.  The results of experiments with the model verified that any form of specified condition results in wave reflection at the boundary which destroys the physical solution. Extrapolation in the form of setting the gradient equal to zero was also shown to be inadequate. The "sponge condition" which is meant to absorb wave energy impinging on the boundary, provided acceptable solutions only if the specified boundary values were consistent with the geostrophically balanced interior. Several formulations of radiation condition (OVER)				
20. DISTRIBUTION/AVAILABILITY OF ABSTRACT  UNCLASSIFIED/UNLIMITED <input type="checkbox"/> SAME AS RPT <input type="checkbox"/> DTIC USERS <input type="checkbox"/>			21. ABSTRACT SECURITY CLASSIFICATION  Unclassified	
22a. NAME OF RESPONSIBLE INDIVIDUAL  Chien-Hsiung Yang			22b. TELEPHONE NUMBER (Include Area Code)	22c. OFFICE SYMBOL  AFGL/LYP

Cont of Block 19:

were tested and the most accurate results were obtained when these were used. The radiation conditions did, however, allow a change of mass within the domain unless the phasespeeds of the outgoing waves were specified exactly.

Tests with initial conditions in which imbalances were present in only the wave number zero fields showed that the model was very slow to respond to this scale of imbalance. This indicates that small errors in the mass variables on the boundaries may not be geostrophically adjusted to the interior very quickly and may not pose a serious problem in short term forecasts. Further, it stresses the importance of initializing a meso-beta model with correctly balanced large scale gradients, even if small scale imbalances remain in the model domain.

# TABLE OF CONTENTS

Introduction	1
One-Dimensional Model	3
Description of the Adjustment Experiments	6
Results Using Fixed or Extrapolated Boundary Conditions	10
a) Boundary Condition Formulations	10
b) Comparison of the Boundary Condition Tests	12
Results Using Radiation Type Boundary Conditions	15
a) Radiation Condition Formulations	15
b) Comparison of the Radiation Condition Tests	18
c. Results Using Averages of the Phasespeeds	21
d) The Higher Order Upstream Scheme (UPHO)	21
Adjustment to Large Scale Imbalances	24
Conclusions and Future Activities	26
References	29



Accession For	
NTIS CRA&I	<input checked="checked" type="checkbox"/>
DTIC TAB	<input type="checkbox"/>
Unannounced	<input type="checkbox"/>
Justification	
By	
Distribution	
Availability Codes	
Dist	Avail and/or Special
A-1	

## 1. Introduction

The specification of prognostic variable values on the lateral boundaries of limited-area numerical models continues to be a serious problem in atmospheric modeling. The computational model requires boundary values where natural atmospheric boundaries do not exist. Theory has provided little guidance in the method of choosing these boundary values. For this reason, lateral boundaries have become an area in which pragmatic experimentation has been the primary source of boundary condition formulation. This is especially true in light of theoretical results which show that, in the general case, it is impossible to formulate truly well-posed boundary conditions (Klemp and Lilly, 1978). A large number of lateral boundary conditions have been formulated and used successfully in various types of atmospheric models. No particular formulation has been shown to be clearly superior, and indeed, the "best" boundary condition is usually determined by the nature of the problem under consideration.

The problem under consideration in this study is the successful modeling of the meso-beta scale with a three-dimensional hydrostatic model. The lateral boundary conditions are particularly crucial on this scale because the model's grid spacing is small enough to resolve



high frequency atmospheric waves (such as internal gravity waves and lee waves) while the time and space scales are large enough to require inclusion of the Coriolis effect. A successful boundary condition must minimize the reflection of outgoing waves by the boundary since the reflected wave energy might destroy the interior solution. The boundary condition must also accurately prescribe the boundary values or else the errors may be geostrophically transmitted to the interior.

A complete discussion of geostrophically adjusted boundary errors was presented by Anthes and Warner (1978). We can think of the mean values of velocity and temperature over the domain in terms of wavenumber zero flow. The mean velocities in the domain are related geostrophically only to gradients of the mass variables across the domain. An error in one of the mass variables on the boundary will imply a change in the large scale gradient and lead to a change in the mean geostrophic velocity in the domain. The mean geostrophic velocity error is proportional to the boundary value error divided by the domain width. Thus, the meso-beta scale should be much more susceptible to this type of error.

This report will present several lateral boundary condition formulations in the context of the meso-beta scale. The emphasis will be on radiation-type conditions

because it will be shown that this type holds the most promise of acceptable results. This study is not meant to represent an exhaustive comparison of boundary condition formulations, but it does provide a comparison of a large number of conditions and especially considers several variations on the radiation condition.

For computational economy, ease of interpretation, and availability of theoretical results, the study reported here concentrates on the use of a one-dimensional, shallow water model to test the various boundary condition formulations. This model filters out many forms of waves important in the atmosphere and cautions about the generality of some of the results obtained will be made at the end of this report. The model provides a good test-bed for the boundary conditions, however, and yields some very important results concerning modeling on the meso-beta scale.

## 2. The One-Dimensional Model

The one-dimensional equations governing the velocities  $u$  and  $v$  and the depth  $\eta$  (see fig. 1) using the shallow water approximation on an  $f$ -plane can be written

$$\frac{\partial}{\partial t}(\eta u) + \frac{\partial}{\partial x}(u \eta u) - f(\eta v) = -\frac{1}{2}g \frac{\partial \eta^2}{\partial x} + \nu \frac{\partial^2}{\partial x^2}(\eta u) , \quad (1)$$

$$\frac{\partial}{\partial t}(\eta v) + \frac{\partial}{\partial x}(u \eta v) + f(\eta u) = \nu \frac{\partial^2}{\partial x^2}(\eta v) , \quad (2)$$

$$\frac{\partial \eta}{\partial t} + \frac{\partial}{\partial x}(\eta u) = 0 , \quad (3)$$

where  $g$  is the acceleration of gravity,  $f$  is the Coriolis parameter, and  $\nu$  is an eddy viscosity. The height-weighted velocities,  $\eta u$  and  $\eta v$ , are analogous to the pressure-weighted velocities used as prognostic variables in many meso-scale hydrostatic models (Anthes and Warner, 1978; Nickerson, 1979) and the continuity equation, (3), is analogous to the pressure tendency equation in a hydrostatic model. In fact, the set (1) through (3) is identical to the equation set which is obtained when a hydrostatic mesoscale model is collapsed to one-dimension along the  $x$ -axis.

We nondimensionalize the equations using the undisturbed height,  $H$ , as a scale. Thus, letting primes denote the nondimensional quantities, we have

$$\begin{aligned}
 \eta &= H \eta' , \\
 u &= \sqrt{gH} u' , \\
 v &= \sqrt{gH} v' , \\
 t &= H/\sqrt{gH} t' = \sqrt{H/g} t' , \\
 x &= H x' , \\
 f &= \sqrt{gH} / H f' = \sqrt{g/H} f' , \\
 \nu &= H\sqrt{gH} K' .
 \end{aligned} \tag{4}$$

Then the nondimensional equations are (dropping primes)

$$\frac{\partial}{\partial t}(\eta u) + \frac{\partial}{\partial x}(u \eta u) - f(\eta v) = -\frac{1}{2} \frac{\partial \eta^2}{\partial x} + K \frac{\partial^2}{\partial x^2}(\eta u) , \tag{5}$$

$$\frac{\partial}{\partial t}(\eta v) + \frac{\partial}{\partial x}(u \eta v) + f(\eta u) = K \frac{\partial^2}{\partial x^2}(\eta v) , \tag{6}$$

$$\frac{\partial \eta}{\partial t} + \frac{\partial}{\partial x}(\eta u) = 0 . \tag{7}$$

Note that  $K$  may now be regarded as an inverse Reynolds number.

The choice of a value for the nondimensional Coriolis parameter determines a relationship between the height scale and the implied latitude. Thus, if a latitude of interest is prescribed, a dimensional length scale must be implicitly chosen even in the nondimensional analysis. We chose to let  $f = 10^{-4} \text{ s}^{-1}$  ( $\phi = 43^\circ \text{Lat}$ ), and choose a height scale  $H = 8 \text{ km}$  (approximately the density scale height). This yields a gravity wave speed of  $\sqrt{gH} = 280 \text{ m/s}$ .

The equations are finite differenced on a staggered grid as shown in fig. 1. Time integration is accomplished with the leapfrog scheme with an Asselin filter (Asselin, 1972) to control timesplitting. The Asselin filter factor is set at 0.5 as suggested by Schlesinger et al. (1983) for the "lagged", weak diffusion used in the model. The normal model domain has 26 grid points for  $\eta$ . A larger domain with 50 grid points for  $\eta$  can also be run. The nondimensional grid spacing is chosen to be  $\Delta x = 2.5$  which corresponds to 20 km. This value, and the resulting domain size of 500 km is typical of meso-beta models. It also assures that all waves resolved in the model satisfy the shallow water assumption on which the equations are based. With the parameter values chosen, a nondimensional time of 1.0 corresponds to 28.6 s. The timestep is chosen to be

$\Delta t = 0.8$ . This is about half the size required for linear stability (including the reduction required by the use of the Asselin filter), but is typical of the value required in a 2-D or 3-D model with the same  $\Delta x$  value. The inverse Reynolds number is set at  $K = 7.813 \times 10^{-3}$  which corresponds to an eddy viscosity of  $1.75 \times 10^4 \text{ m}^2/\text{s}$ . The model has been coded with a variety of lateral boundary conditions. These will be described in the following sections along with the results of each type of condition.

### 3. Description of the Adjustment Experiments

The major concern of most lateral boundary condition formulations is their ability to allow waves generated in the domain to exit (or be absorbed) without reflection. If this is accomplished, the lateral boundary will appear transparent and allow the limited area model to better represent the unbounded region it is simulating. Another concern is the possibility of errors in the large scale gradients implied by the boundary values being geostrophically adjusted throughout the domain. On the meso-beta scale, temperatures and windspeeds must be specified with errors of less than about  $1^\circ\text{C}$  and  $2 \text{ m/s}$ , respectively, in order to give acceptable geostrophically adjusted interior errors (Anthes and Warner, 1978).

A major source of waves in the domain during a

simulation is the geostrophic adjustment of imbalances between the dynamic fields. In general, at the start of the integration, the velocity and mass fields will not be in perfect gradient balance and gravity and Lamb waves will be generated during the adjustment process. These waves radiate away from the imbalance to leave behind a balanced state. If the lateral boundary conditions of a numerical model reflect some or all of the wave energy back into the interior, the reflected waves will unrealistically influence the simulated solution, interfering with the balance and prohibiting the adjustment process.

In this study, experiments were conducted with two different types of initial imbalances as initial conditions. Initial condition 1 is a perturbation in the height field and initial condition 2 is an imbalanced local wind. The scale of these imbalanced regions is smaller than the domain size of the model (500 km) and therefore much smaller than the Rossby radius of deformation ( $\lambda = C/f = 2.8 \times 10^3$  km). Theory predicts that the pressure should adjust to the winds with the wind field remaining essentially unchanged.

Each of these two initial conditions were run in the large domain model in order to determine their natural evolution during adjustment. For these simulations, the model used a radiation lateral boundary condition with the phasespeed set to the analytical value of  $C = 1.0$ . This

will be shown to be the least reflective formulation.

The first imbalance (initial condition 1) is a perturbation in height only with the velocities set to zero. The initial height field and its evolution are shown in fig. 2. The perturbation is a height deficit of 0.3 % (comparable to a pressure deficit of 3 mb) in the center of the domain. Height excesses are located on either side of the deficit so that the equilibrium height is  $\eta = 1.0$ . As linear shallow water theory would predict, the evolution of this disturbance is for two deficit waves to propagate in opposite directions at the shallow water wavespeed,  $C = \pm 1.0$ , leaving a (trivially) balanced state behind. The Coriolis effect plays little role in this adjustment as indicated by a simulation with  $f = 0$  (not shown) which yielded essentially identical results. The primary velocities are in the  $u$  component due to the height gradient. Small values of  $v$  are accelerated geostrophically as the first half of the wave passes a point. However, these are quickly diminished as the sign of the acceleration changes during the passage of the rest of the wave. Note that by  $t = 72$ , the wave is no longer present in the area covered by the small domain and the height field is level.

In the second adjustment experiment, the height field is initially specified as  $\eta = 1.0$ , but a limited jet is imposed in  $v$  with  $u$  initially zero. This is essentially the

geostrophic adjustment problem studied by Cahn (1945) using a linear shallow water model. The  $t = 0$  frame of fig. 3 shows the extent of the jet, which was set at  $v = 10$  m/s (dimensionally). The remainder of the figure shows the evolution of the height field. As predicted by linear theory, the height field adjusts to the imbalance by producing a wave of excess which moves to the right and a wave of deficit which moves to the left. The resulting height field has a height gradient in geostrophic balance with the velocity in the region of the jet and a constant height in balance with the zero velocities away from the jet. Note that, unlike initial condition 1, the balanced state requires final boundary values to be different from their initial values. Also note that while the Coriolis effect plays little role in the evolution of initial condition 1, it is essential to the evolution shown in fig. 3. If  $f = 0$ , the  $v$  component is decoupled from the other variables in equations (1) through (3) and no adjustment would be necessary.

In the following sections, specific lateral boundary condition formulations will be described and the results of tests using these conditions in the one-dimensional model will be presented. All boundary conditions were tested with both initial conditions. In the figures which allow comparison of the boundary conditions, the height field



labeled "LD" is the large domain's center 26 grid points and may be thought of as the "exact" solution. Each boundary condition formulation will be denoted with a three or four letter descriptor (such as FXD for fixed conditions) as is used in the figures.

#### 4. Results Using Fixed or Extrapolated Boundary Conditions

##### a) Boundary Condition Formulations

1) Fixed boundary condition (FXD). This boundary condition consists simply of specifying boundary values initially and holding these values constant throughout the integration. It may be written

$$\frac{\partial \phi}{\partial t} = 0 , \quad (8)$$

where  $\phi$  is any prognostic variable ( $\eta$ ,  $u$ , or  $v$  in the present model). This approach eliminates the potential problem of geostrophically adjusted boundary errors, provided the initial boundary values are correctly chosen. This boundary condition is not mathematically well-posed, however, in that it results in an overspecification of the problem. It also is purely reflective of waves generated in the domain's interior.

2) Combination of fixed and extrapolated (FEX). In order to allow the boundary to be more "open", while

still controlling geostrophically adjusted errors, some mesoscale models use fixed conditions on some variables while extrapolating others (Anthes and Warner, 1978; Nickerson, 1979). The typical approach is to fix the pressure and thermodynamic variables and set the horizontal gradients of the velocities equal to zero (Anthes and Warner, 1978). Here, the formulation follows Nickerson (1979) with the height specified and the velocities extrapolated only when the flow is outward. That is

$$\begin{aligned} \frac{\partial \eta}{\partial t} &= 0, \\ \left\{ \begin{array}{ll} \frac{\partial u}{\partial x} = \frac{\partial v}{\partial x} = 0 & \text{for } u \text{ outward,} \\ \frac{\partial u}{\partial t} = \frac{\partial v}{\partial t} = 0 & \text{for } u \text{ inward.} \end{array} \right. \end{aligned} \quad (9)$$

3) Zero-gradient condition (GRD). This condition extrapolates all variables on the boundary by specifying the horizontal gradient to be zero. This may be written

$$\frac{\partial \phi}{\partial x} = 0, \quad (10)$$

where  $\phi = \eta, u, \text{ or } v$ . This condition is implemented by setting the boundary value equal to the value one grid point interior to the boundary at each timestep.

4) Sponge condition (SPG). This condition follows the formulation of Perkey and Kreitzberg (1976). The

boundary values are specified and do not change in time. However, the time tendencies at the gridpoints are modified such that

$$\frac{\partial \phi}{\partial t} = W(I) \frac{\partial \phi}{\partial t} , \quad (11a)$$

where

$$W(I) = \begin{cases} 0.0 & \text{for } I = \text{boundary grid points} \\ 0.4 & \text{for } I = \text{boundary-1 grid points} \\ 0.7 & \text{for } I = \text{boundary-2 grid points} \\ 0.9 & \text{for } I = \text{boundary-3 grid points} \\ 1.0 & \text{for all interior grid points} \end{cases} \quad (11b)$$

This type of boundary condition absorbs waves by reducing their phase speed to zero as they approach the boundary (Perkey and Kreitzberg, 1976). As the phasespeed is reduced, the wavelength also becomes smaller. This adds energy to  $2 \Delta x$  waves. Therefore, a filter of some sort is required. A fourth-order diffusion term is used in this study to remove this  $2\Delta x$  energy.

#### b) Comparison of the Boundary Condition Tests

Figures 4 and 5 show the height field in comparative test results for initial condition 1 at the nondimensional times  $t = 36$  and  $t = 72$ , respectively. The height field labeled LD is the center 26 grid points of the large domain model and may be thought of as the solution resulting from truly open lateral boundaries. It is clear that all of the

boundary conditions shown here have serious problems with reflection of the outward propagating waves.

The fixed and fixed/extrapolated (FXD and FEX) conditions produced nearly identical results. This suggests that extrapolation of only the velocities does not allow the boundary to be more open to the outgoing wave. Extrapolation of all the variables through the zero-gradient condition (GRD) is not adequate either. However, this condition appears to produce errors of comparable magnitude (though of different phase). The sponge condition, while the best of this set of conditions, fails to completely absorb the wave. This may be a result of the small number of gridpoints in the model (which is typical of the number of grid points in one direction in a 3-D model). It may also be a result of the relatively rapid phasespeed of the wave in this model. Tests of the sponge condition reported by Perkey and Kreitzberg (1976) which showed nearly completed absorption involved internal gravity waves which required many timesteps to traverse the width of the sponge.

A similar comparative display for initial condition 2 at times  $t = 36$  and  $t = 72$  is shown in figures 6 and 7. It is impossible for any of the boundary conditions which hold the boundary value fixed (FXD, FEX, SPG) to achieve the balanced final state. This leads to a very disturbed solution as the initial jet in the  $v$  component continually

forces a height gradient but the reflection of the waves generated interferes with the height field adjustment. The only acceptable balanced final state for these conditions is for the jet in  $v$  to be diminished to zero. Since the geostrophic adjustment on this scale is made by the height field, however,  $v$  is only diminished by the small viscosity in the model.

The zero-gradient condition (GRD) which is not constrained by fixed endpoint values appears initially to be allowing the adjustment to proceed with only small errors. At  $t = 36$ , the height gradient in the jet region is approximately correct. We can see also that the endpoints have adjusted in the right sense, although they are further from the equilibrium height than they should be. However, by  $t = 72$ , it is clear that this condition is not handling the adjustment properly.

Again, the sponge condition appears to yield the best results despite the specified values on the endpoints. The condition tends to concentrate the imbalance in the sponge region near the boundaries and maintains a partial adjustment in the interior. While not ideal, this condition could be considered adequate in many situations, especially if the initial conditions contained only small imbalances.

## 5. Results Using Radiation Type Boundary Conditions

### a) Radiation Condition Formulations

Radiation type lateral boundary conditions are based on the Sommerfeld radiation condition

$$\frac{\partial \phi}{\partial t} + C \frac{\partial \phi}{\partial x} = 0 , \quad (12)$$

where  $\phi$  is the variable of interest on the boundary and  $C$  is the phasespeed of the outgoing wave. Variations in the radiation condition formulation arise from the various methods that can be used to specify the phasespeed,  $C$ , and to finite difference the equation. For the shallow water model, all waves move at the shallow water wavespeed, so  $C = 1.0$  exactly. In the general case, however, the wavespeed is not known and must either be calculated from information available in the interior, or specified at some reasonable value. Klemp and Lilly (1978), for example, specified the phasespeed as the expected internal gravity wavespeed calculated from the environmental stability. However, Clark (1979) showed that a calculated variable phasespeed gave less reflection. Most studies using radiation conditions have used a variable  $C$ . We will consider several variable phasespeed formulations.

In all the radiation condition formulations,  $C$  is required to satisfy the Courant-Friedrichs-Levy (CFL)

condition. In addition, if  $C$  is calculated to be inward, it must be set equal to zero to prevent spurious generation of waves. Thus,  $C$  must satisfy

$$C = \begin{cases} 0 & \text{for } C \text{ inward} \\ C & \text{for } 0 < C < \Delta x / \Delta t \\ \Delta x / \Delta t & \text{for } C > \Delta x / \Delta t \end{cases} \quad (13)$$

Note that for  $C = 0$ , (12) reduces to  $\partial\phi/\partial t = 0$  for that timestep.

1) Orlanski-type centered on previous timestep (ORP). This is the original formulation by Orlanski (1976). It calculates  $C$  by inverting (12) and evaluating  $\partial\phi/\partial t$  and  $\partial\phi/\partial x$  at the previous timestep and one grid point interior to the boundary. Then

$$C = -\frac{\partial\phi}{\partial t} \left[ \frac{\partial\phi}{\partial x} \right]^{-1}, \quad (14)$$

where

$$\frac{\partial\phi}{\partial t} = \frac{1}{2\Delta t} [\phi_{b-1}^{\tau} - \phi_{b-1}^{\tau-2}], \quad (15)$$

and

$$\frac{\partial\phi}{\partial x} = \frac{1}{\Delta t} \left[ \frac{1}{2} (\phi_{b-1}^{\tau} + \phi_{b-1}^{\tau-2}) - \phi_{b-2}^{\tau-1} \right]. \quad (16)$$

In the above,  $\phi_{b-i}$  is the  $i$ th grid point interior to the boundary and the superscript denotes the timestep. The term in parenthesis in (16) is used to prevent timesplitting on the boundary point. The new boundary value is then given by

$$\phi_b^{\tau+1} = \frac{(1 - C\Delta t/\Delta x)}{D} \phi_b^{\tau-1} + \frac{2C\Delta t/\Delta x}{D} \phi_{b-1}^{\tau}, \quad (17)$$

where  $D = 1 + C \Delta t/\Delta x$ .

2) Orlanski-type centered on current timestep (ORC).

As suggested by Raymond and Kuo (1984), when an explicit time scheme is used in a model, the calculation of  $C$  can be centered on the current timestep. Then the calculation of  $C$  is identical to (14) through (16) with  $\tau$  replaced by  $\tau + 1$ . The boundary value calculation is still identical to (17).

3) Upstream technique (UPS). Bannon (1979) and Miller and Thorpe (1981) have both proposed using upstream differencing to evaluate the radiation equation (12). Inverting the equation to obtain  $C$  then gives

$$C = -\frac{\partial \phi}{\partial t} \left[ \frac{\partial \phi}{\partial x} \right]^{-1}, \quad (18)$$

as before, but now

$$\frac{\partial \phi}{\partial t} = \frac{1}{\Delta t} [\phi_{b-1}^{\tau} - \phi_{b-1}^{\tau-1}] \quad (19)$$

and

$$\frac{\partial \phi}{\partial x} = \frac{1}{\Delta x} [\phi_{b-2}^{\tau} - \phi_{b-1}^{\tau}] \quad (20)$$

The boundary point is then given by

$$\phi_b^{\tau+1} = \phi_b^{\tau} - C \frac{\Delta t}{\Delta x} [\phi_b^{\tau} - \phi_{b-1}^{\tau}] \quad (21)$$



4) Radiation conditions with the exact phasespeed (ORE and UPE). For the shallow water model, the exact phasespeed is known ( $C = 1.0$ ) so this value may be used in the radiation condition to isolate errors resulting from the finite difference representation alone. When the exact phasespeed is used, ORP and QRC become identical and this form is denoted ORE. The upstream form, UPS, is denoted UPE when the exact phasespeed is used. This approach is useful in the present study, but is not applicable in a more general model which admits waves of different phasespeeds.

b. Comparison of the Radiation Condition Tests

Figures 8 and 9 show a comparison of the radiation condition formulations for initial condition 1 at nondimensional times  $t = 36$  and  $t = 72$ . Again, the LD solution may be thought of as giving an exact boundary value. We find here that all of the radiation condition formulations yield superior results to the boundary conditions used to produce figures 4 and 5. Differences between the individual radiation conditions are most apparent at  $t = 72$  (fig. 9).

Clearly, the conditions using the exact phasespeed are the best (ORE and UPE). However, even these result in a slight reflection of wave energy. This reflection is due to

the finite differencing of (12) and shows that even perfect calculation of  $C$  in a more general model will result in a small error at the boundary. This result is also noted in the formal analysis carried out by Miller and Thorpe (1981).

An important and very noticable point in the three variable phasespeed formulation results (ORP, ORC, and UPS) is that the height field has dropped below the equilibrium level of  $\eta = 1.0$  at  $t = 72$ . This indicates that mass has been lost through the open boundaries as waves exited. This is a potentially serious problem which could adversely affect the performance of a more complicated atmospheric model. This is clearly related to the variable phasespeed since the exact phasespeed results do not exhibit a noticable change in mass.

The flux of mass through the boundaries appears to be related to two factors. First, the phasespeeds used in the radiation condition are calculated seperately for each variable. Despite the strength and coherence of the waves generated by initial condition 1, the calculated phasespeeds bear little resemblance to the theoretical ideal. Fig. 10 shows the phasespeeds calculated by ORP for each of the three variables as a function of time. As can be seen, they oscillate wildy between zero and CFL limit. Further, there is little relation between the phasespeeds calculated for the different variables. This can lead to boundary

tendencies which are not consistent with continuity of mass and a resulting mass flux through the boundary. Plots of the phasespeeds versus time for ORC and UPS show similar characteristics.

The second factor which appears to be important in the flux of mass through the boundary is the nature of the staggered grid. The boundary gridpoints on which the velocities are modified by the boundary condition are one half grid spacing outward from the boundary points for height. Thus, even if all three variables use the same value of  $C$ , this value is being used at different spatial points on the wave. Thus, unless  $C$  is calculated perfectly at every timestep, different parts of the wave will be advected at different speeds through the boundary, resulting in a net mass flux. Results obtained using averages of  $C$ , which demonstrate this conclusion, will be shown in the next section.

Figures 11 and 12 show the performance of the radiation conditions on initial condition 2 at  $t = 36$  and  $t = 72$ . Since the boundary values are able to evolve naturally in time, all of the radiation condition formulations allow a natural adjustment to take place. Again, ORE and UPE give the best results, but all of the formulations give satisfactory results. There was little evidence of a change in mass in the experiments using initial condition 2.

### c. Results Using Averages of the Phasespeeds

As can be seen in fig. 10, while the individual phasespeeds calculated for each variable oscillate wildly, an average of them would tend to be closer to  $C = 1.0$ . Each of the radiation condition formulations was tested with the phasespeed being the average of the phasespeeds calculated using  $\eta$ ,  $u$ , and  $v$  alone. These versions of ORP, ORC, and UPS are denoted ORPA, ORCA, and UPSA, respectively. The phasespeed as a function of time for ORPA using initial condition 1 is shown in fig. 10 as the heavy solid line. Note that this is not exactly the same as the average of the individual phasespeeds from ORP because the evolution of the flow in ORPA is modified. As anticipated, the phasespeed in ORPA (as well as in ORCA and UPSA which are not shown but similar) remained closer to the analytic phasespeed,  $C = 1.0$ .

Figures 13 and 14 show the height field for initial conditions 1 and 2 at  $t = 72$  for the radiation conditions using the average phasespeed. These results are somewhat closer to the results obtained with the analytic phasespeed. It is evident in fig. 13 that there is still a mass flux through the boundary. Now, however, the mass of the domain is increasing rather than decreasing.

### d. The Higher Order Upstream Scheme (UPH0)

Miller and Thorpe (1981) presented a radiation

condition formulation using upstream differencing which has a formal accuracy of higher order than ORP, ORC, or UPS. The model results using this condition (denoted UPHO) with initial conditions 1 and 2 are shown in figures 13 and 14, respectively. As can be seen, this condition does not allow the waves to exit the domain without reflection. Since this condition is formally more accurate than the previously discussed radiation conditions, its relatively poor performance is somewhat surprising. Raymond and Kuo (1984) tested this higher order scheme in a two-dimensional model and also found it to give unsatisfactory results. This section will outline the formulation of this condition and seek to explain why its practical accuracy is far less than its formal accuracy.

Following the notation of Miller and Thorpe (1981) we can let  $r = C \Delta t / \Delta x$  be a nondimensional phasespeed. The CFL and outflow conditions reduce to  $0 < r < 1$  (for  $r$  positive on outflow). Then the normal upstream calculation of the phasespeed given by equations (18) through (20) may be written

$$r_u = [\phi_{b-1}^{\tau} - \phi_{b-1}^{\tau-1}] [\phi_{b-2}^{\tau-1} - \phi_{b-1}^{\tau-1}]^{-1}, \quad (22)$$

which can be shown to be of second order accuracy (Miller and Thorpe, 1981). Two other possible calculations of  $r$  are

given by

$$r_1 = [\phi_{b-1}^{\tau+1} - \phi_{b-1}^{\tau}] [\phi_{b-2}^{\tau} - \phi_{b-1}^{\tau}]^{-1}, \quad (23)$$

and

$$r_2 = [\phi_b^{\tau} - \phi_b^{\tau-1}] [\phi_{b-1}^{\tau-1} - \phi_b^{\tau-1}]^{-1}. \quad (24)$$

Miller and Thorpe (1981) then show that the proper combination of these three, given by

$$r = r_1 + r_2 - r_0 \quad (25)$$

achieves a formal truncation error which is third order. Thus, this combination should give higher accuracy. To implement this condition, we find  $r$  using equations (22) through (25), then let  $C = r \Delta x / \Delta t$  and use equation (21) to update the boundary value.

Extensive testing with the one-dimensional model has confirmed a rather simple explanation for the poor performance of this condition. The calculations of  $r_0$  and  $r_1$  both rely on an upstream difference at a point one grid spacing interior to the boundary, and differ only in the timestep on which the calculation is based. For an existing wave which requires several timesteps to pass through the boundary, both  $r_0$  and  $r_1$  would be expected to give similar results. The calculation of  $r_2$ , however depends on a time difference on the boundary point itself. Therefore,  $r_2$  is coupled to the boundary condition itself and will yield a

nonzero result only when the boundary condition allows a change in the boundary value. If the boundary value has not changed in two timesteps,  $r_2 = 0$ , and  $r = r_1 - r_u$ . But  $r_1 \approx r_u$ , so their difference will be approximately zero and may be negative. A negative  $r$  indicates inflow (assuming  $r$  positive on outflow), so  $r$  is set to zero and the boundary value is not modified. This feedback maintains  $r_2 = 0$  and results in essentially fixed conditions with the resulting reflection. In the simulations made using UPHO, brief periods on nonzero  $r$  interrupted longer periods when the condition set  $r$  to zero. Thus, for some brief periods of the integration, waves were able to exit the domain.

## 6. Adjustment to Large Scale Imbalances

The results for initial conditions 1 and 2 described above involve geostrophic adjustment of imbalances on scales smaller than the Rossby radius of deformation. In these cases, the height field adjusts to the winds. The model's response to imbalances in the large scale ("wavenumber zero") fields yields results of importance to both model initialization and lateral boundary condition formulation. Even though the model domain is smaller than the radius of deformation, a constant gradient of height which is out of balance with a constant wind will be treated by the model as an infinitely large disturbance. In this case, theory

predicts that the winds should adjust to the pressure.

One experiment involved initializing the model with a constant height gradient which would be in geostrophic balance with a  $v$  velocity of 2 m/s. The initial  $v$  component was set to zero, however, so the fields were out of balance. The adjustment process in this case is fairly clear from a consideration of equations (1) through (3). The height gradient accelerates a  $u$  velocity (from (1)) which in turn accelerates a  $v$  velocity (from (2)). As  $v$  becomes larger and approaches geostrophic balance with the height gradient, the acceleration of  $u$  is diminished and eventually  $u$  is decelerated to zero leaving only the geostrophically balanced  $v$  component and height gradient. Simulations with the one-dimensional model show this adjustment process to be an order of magnitude slower than the adjustment of a localized disturbance. By the nondimensional time  $t = 240$ , the  $v$  component had been accelerated to a dimensional value of only 0.44 m/s. Other simulations using a variety of large scale imbalanced initial conditions have confirmed this slow adjustment process.

This result indicates that it is very important for the large scale gradients to be very close to balance in an atmospheric model's initialization. The local imbalances due to topography or higher resolution data present in the initialization will balance quickly provided an appropriate



lateral boundary condition is used. Imbalances in the large scale gradients, however, will adjust in a time scale comparable to the inertial period ( $\sim 17$  hours).

This result also indicates that the concern of Anthes and Warner (1978) about geostrophically adjusted boundary value errors is not warranted in meso-beta models, which typically make forecasts for periods much shorter than one day. However, it may still be important for larger scale models which forecast for a day or more. The adjustment process is sufficiently slow that errors produced by the boundary conditions will require several hours to significantly affect the mean geostrophic flow in the interior. In choosing lateral boundary conditions for meso-beta models, then, emphasis should be placed on the ability of the condition to deal with waves generated in the interior of the domain by natural processes or the geostrophic adjustment of initial local imbalances.

## 7. Conclusions and Future Activities

This report has discussed the test results lateral boundary conditions in a one-dimensional shallow water model. The results show conclusively that radiation conditions allow waves to exit the domain without serious reflection and allow the boundary points to evolve with the geostrophic adjustment of the interior so that a balanced

state may be reached. Of the non-radiation type conditions tested, only the sponge condition of Perkey and Kreitzberg (1976) showed signs of being adequate, though still inferior. One of the primary reasons for choosing the sponge condition or some other fixed boundary value condition, has been the concern of geostrophically adjusted large scale gradient errors due to the boundary condition (Anthes and Warner, 1978). This has been shown to be of secondary importance on the meso-beta scale. A potential problem with radiation conditions, however, is the flux of mass through the lateral boundary which may result in a total change in mass for the domain. This problem is reduced if the phasespeeds are calculated accurately.

The analysis of lateral boundary conditions using a one-dimensional model does not replace boundary condition testing in a full three-dimensional model. It does, however, compliment it. The one-dimensional modeling allows a large number of variations of boundary conditions to be tested economically. Further, since the one-dimensional model equations are much simpler than the three-dimensional set, physical interpretation of the results is much simpler. The price of this simplification is that some types of motion (such as internal gravity waves) may be filtered out, so the easy physical interpretation in the one-dimensional case may not always extend to the three-dimensional model

results. Thus, it is useful to use both approaches. The one-dimensional model can eliminate obviously inadequate boundary conditions and test minor variations in the reasonable ones, and the three-dimensional model can test the most promising candidates revealed from the one-dimensional tests.

Some experiments using fixed/extrapolated, sponge, and radiation conditions have been carried out with the full three-dimensional model. These tests have basically supported the results presented in this report. Future work will involve further testing in the three-dimensional model. Work will also continue with the one-dimensional model. This will involve the inclusion of time dependent data on the lateral boundaries which is important for meso-beta models nested in larger scale models.

## References

- Anthes, R.A., and T.T. Warner, 1978: Development of hydrodynamic models suitable for air pollution and other mesometeorological studies. Mon. Wea. Rev., 106, 1045-1078.
- Asselin, 1972: Frequency filter for time integration. Mon. Wea. Rev., 100, 487-490.
- Bannon, P.R., 1979: On the dynamics of the East African jet. Ph. D. Thesis, University of Colorado.
- Cahn, A., 1945: An investigation of the free oscillations of a simple current system. J. Met., 2, 113-119.
- Clark, T.L., 1979: Numerical simulations with a three-dimensional cloud model: Lateral boundary condition experiments and multi-cellular severe storm simulations. J. Atmos. Sci., 36, 2191-2215.
- Klemp, J.B., and D.K. Lilly, 1978: Numerical simulation of hydrostatic mountain waves. J. Atmos. Sci., 35, 78-107.
- Miller, M., and Thorpe, A., 1981: Radiation conditions for the lateral boundaries of limited-area numerical models. Quart. J. R. Met. Soc., 107, 615-628.
- Nickerson, E.C., 1979: On the simulation of airflow and clouds over mountainous terrain. Beit. Atmos. Phys., 52, 161-177.
- Orlanski, I., 1976: A simple boundary condition of unbounded hyperbolic flows. J. Comp. Phys., 21, 251-269.
- Perkey, D.J., and C.W. Kreitzberg, 1976: A time-dependant lateral boundary scheme for limited-area primitive equation models. Mon. Wea. Rev., 104, 744-755.
- Raymond, W.H., and H.-L. Kuo, 1984: A radiation boundary condition for multi-dimensional flow. Quart. J. R. Met. Soc., 110, 535-551.
- Schlesinger, R.E., L.W. Uccellini, and D.R. Johnson, 1983: The effects of the Asselin time filter on numerical solutions to the linearized shallow water wave equations. Mon. Wea. Rev., 455-467.



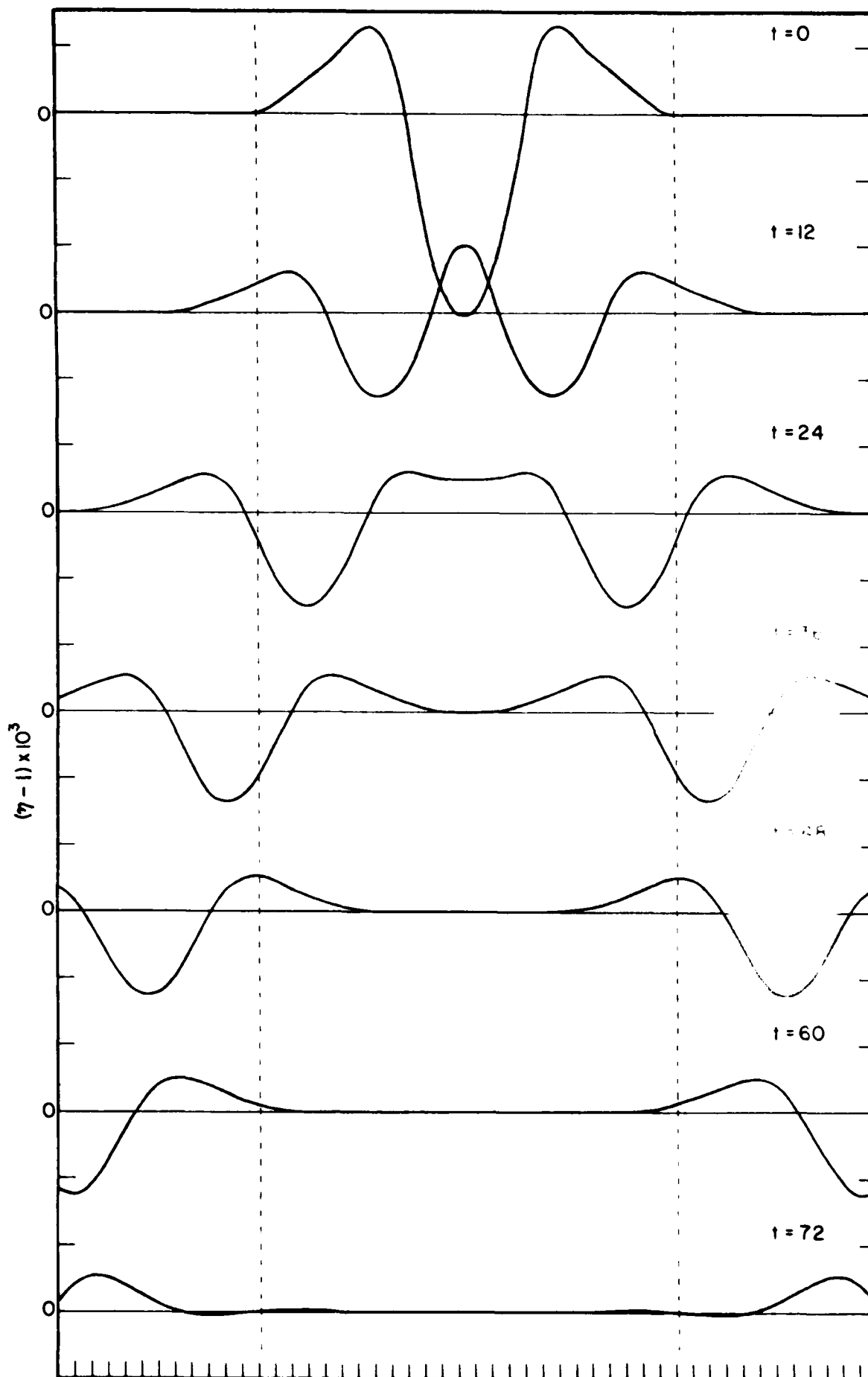


Figure 2. Evolution of initial condition 1 in the large domain model. Tick marks along the bottom show the location of grid points, and the dashed lines indicate the location of endpoints in the 26 gridpoint model.

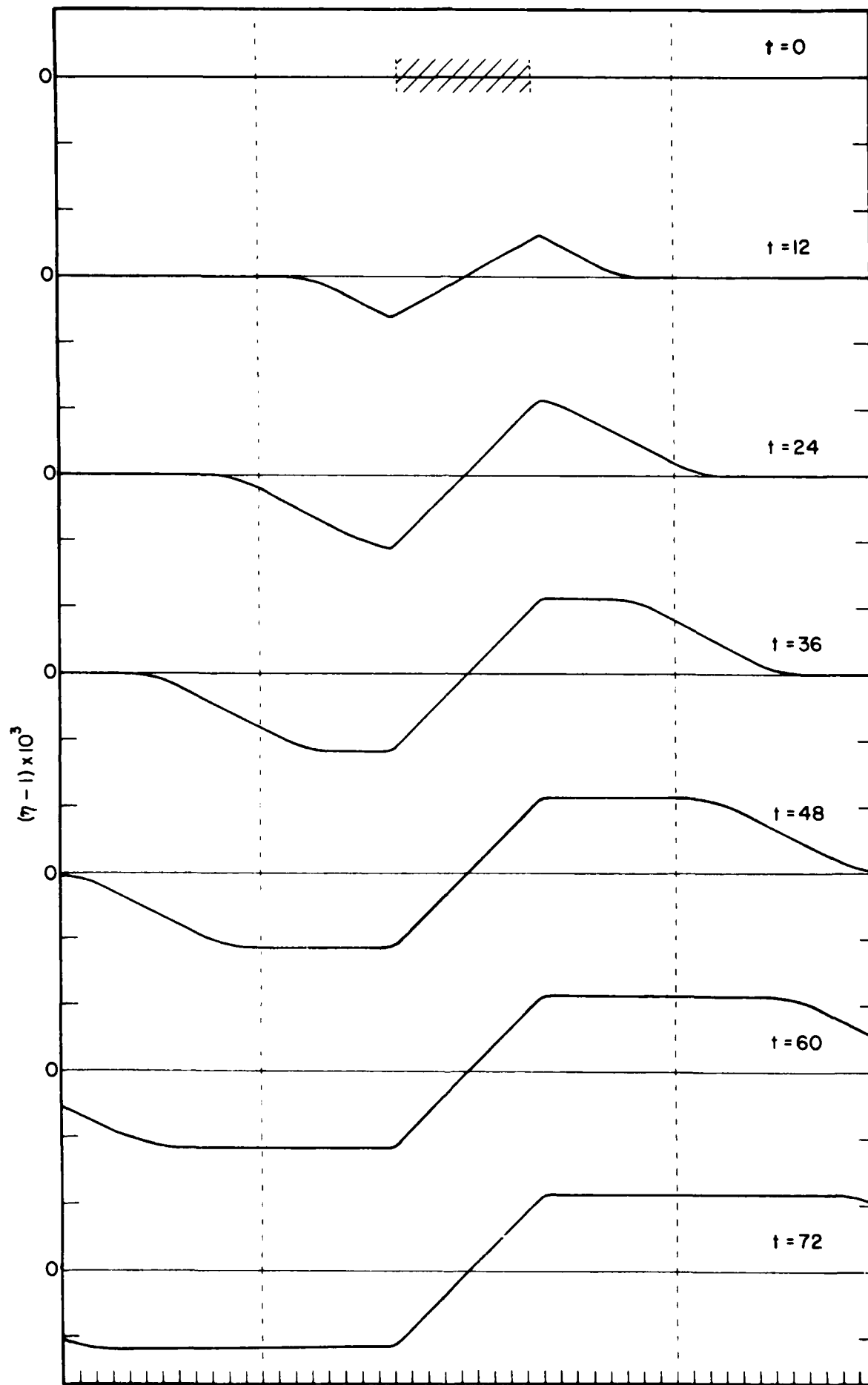


Figure 3. As fig. 2 for initial condition 2. The hatched region at  $t = 0$  indicates the extent of the initial velocity jet.

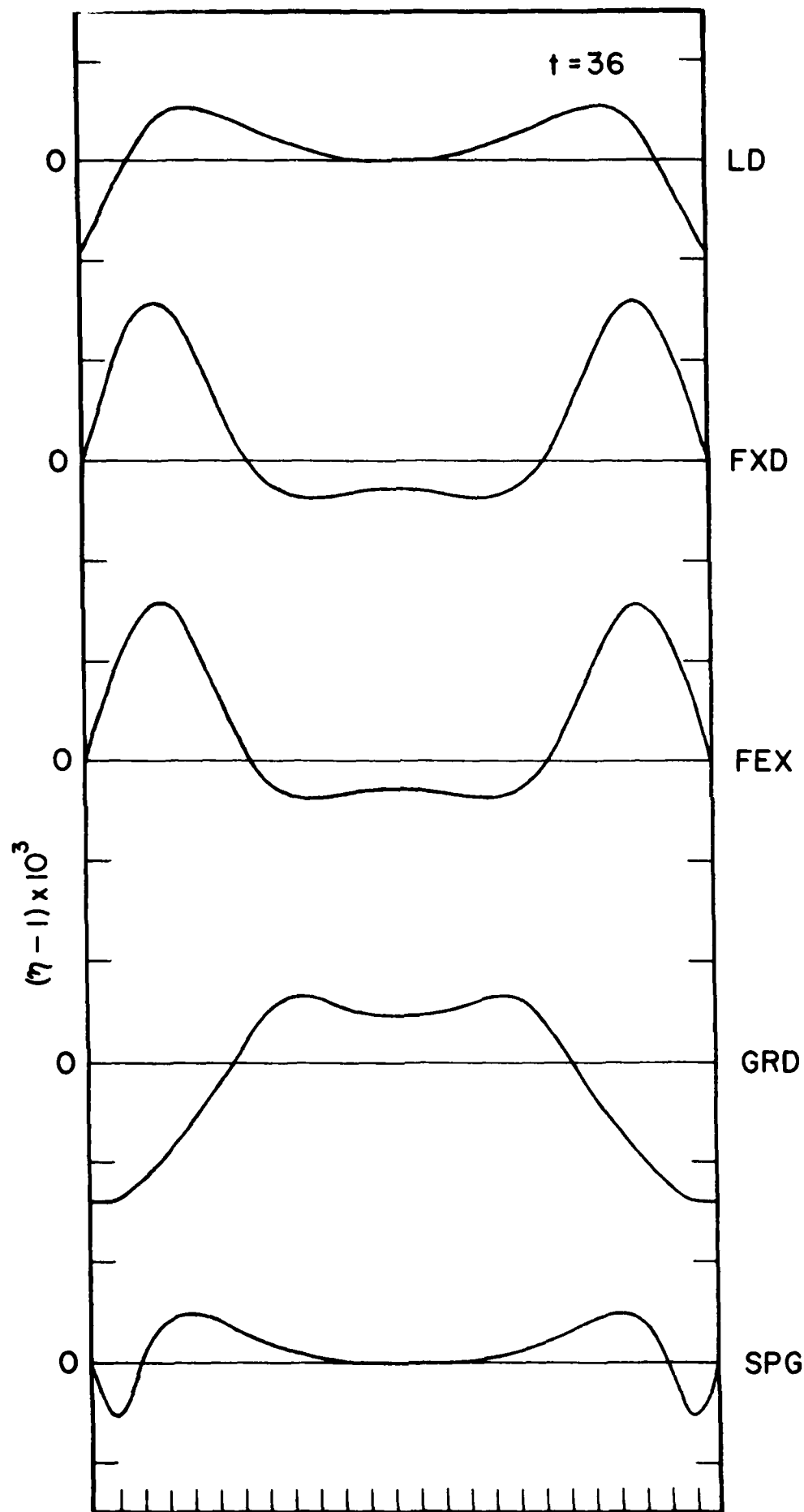


Figure 4. Comparison of the height field at  $t = 36$  using the indicated boundary conditions in the 26 gridpoint model with initial condition 1.



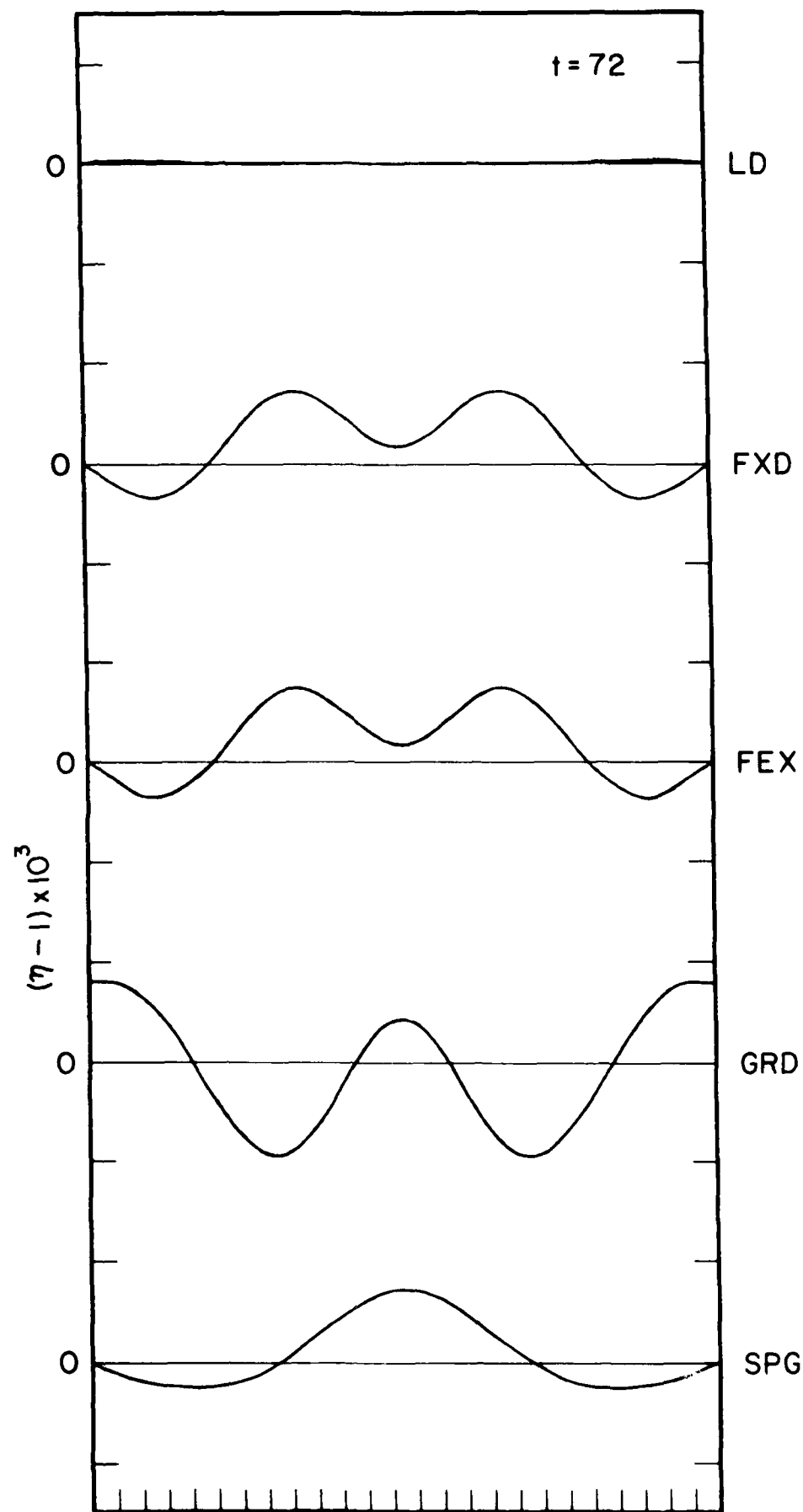


Figure 5. As fig. 4 at  $t = 72$ .

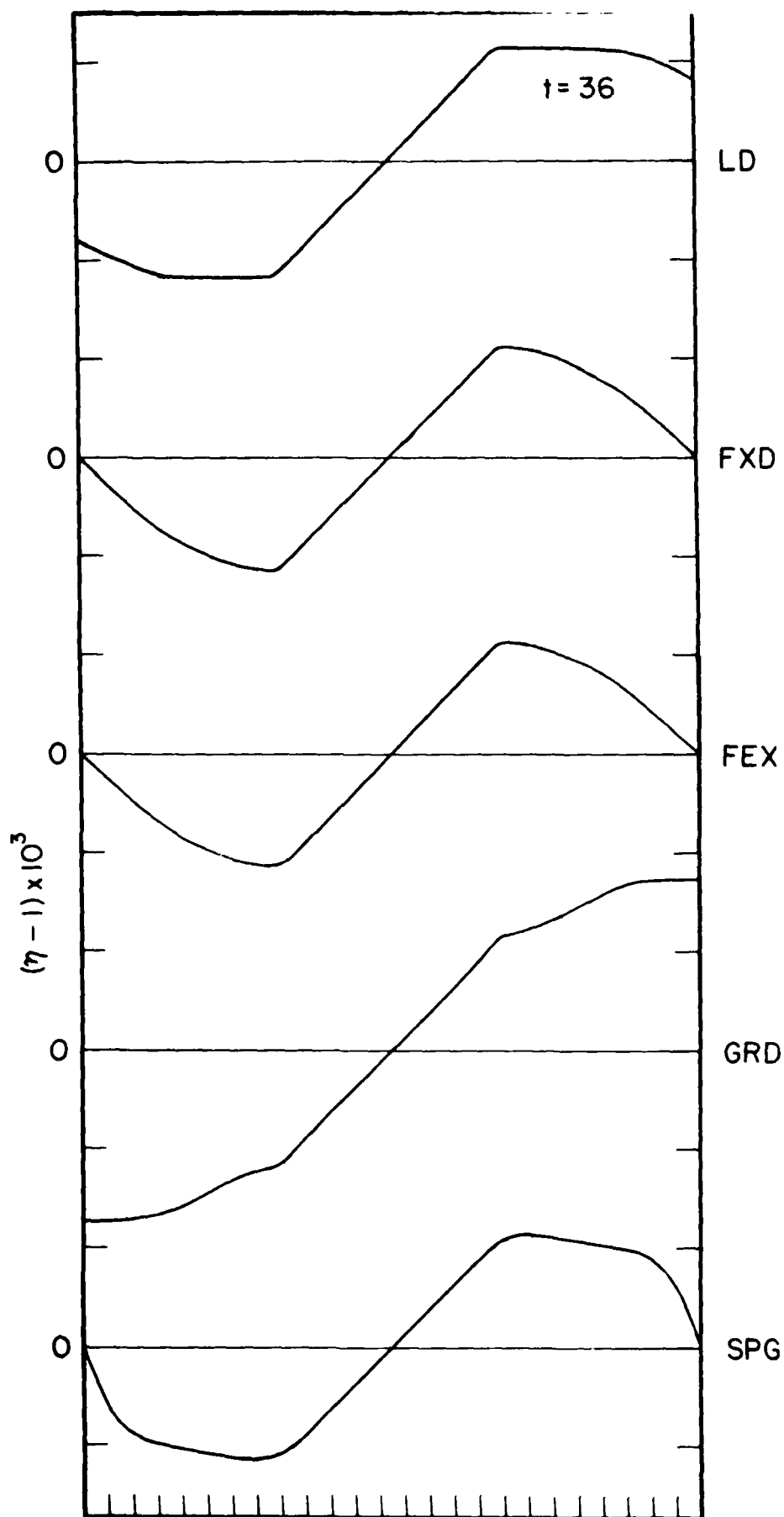


Figure 6. As fig. 4 for initial condition 2.

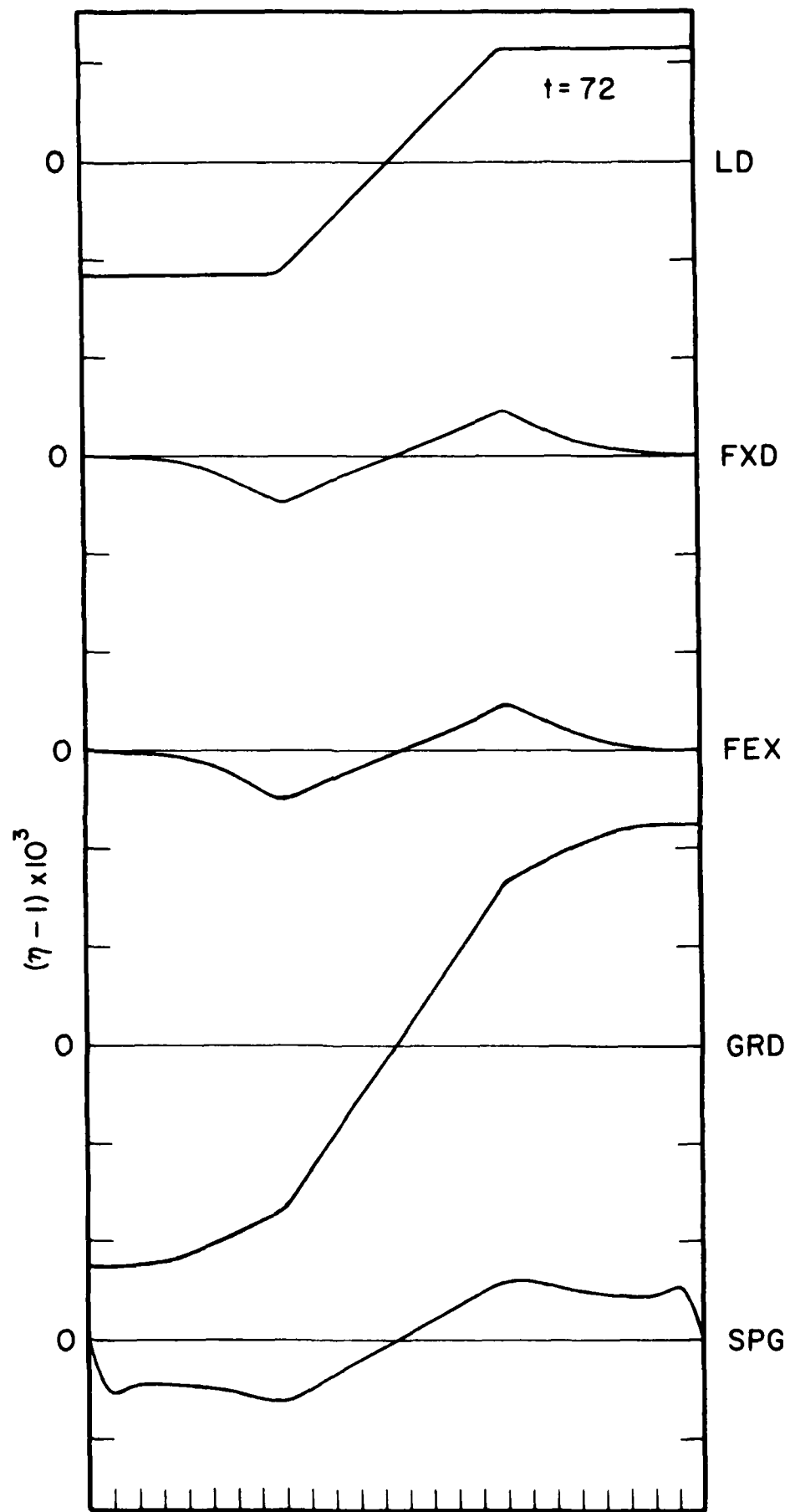


Figure 7. As fig. 4 at  $t = 72$  for initial condition 2.

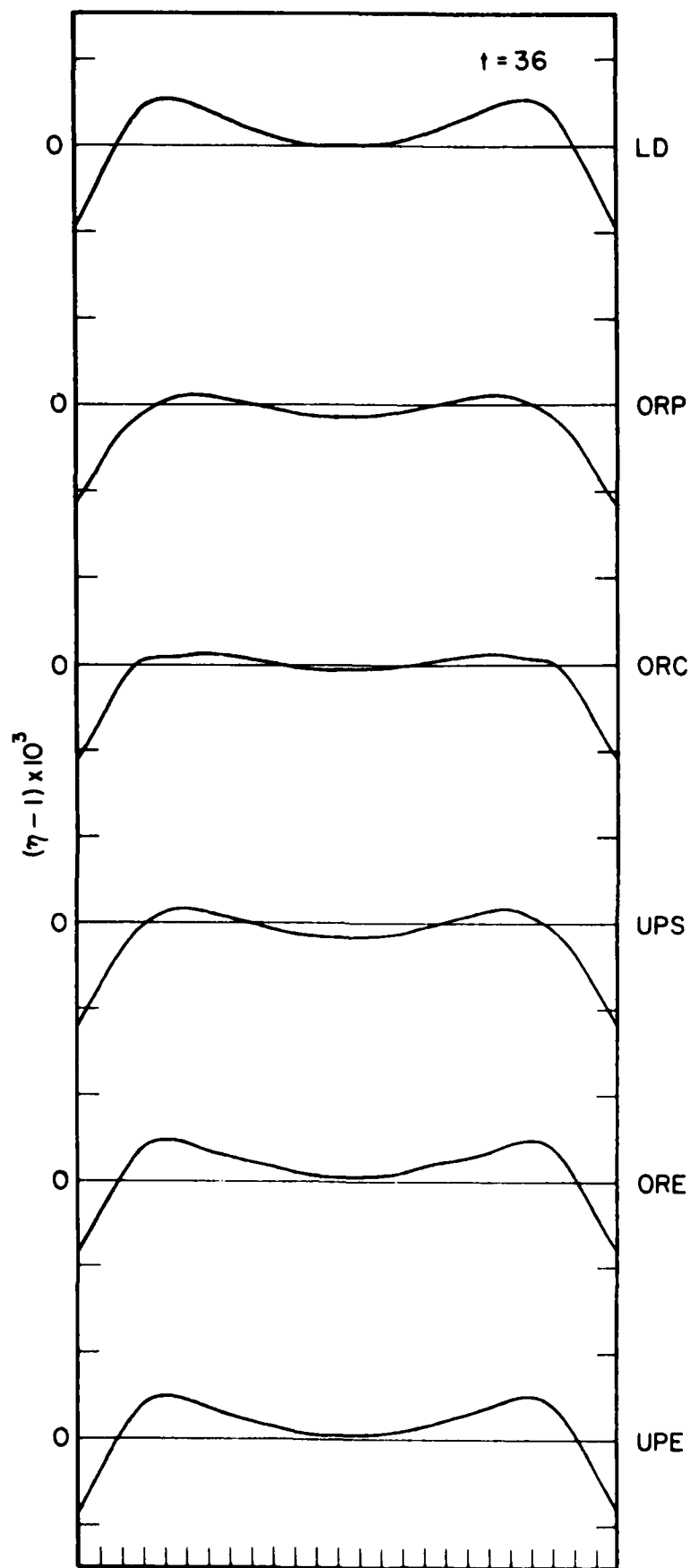


Figure 8. As fig. 4.

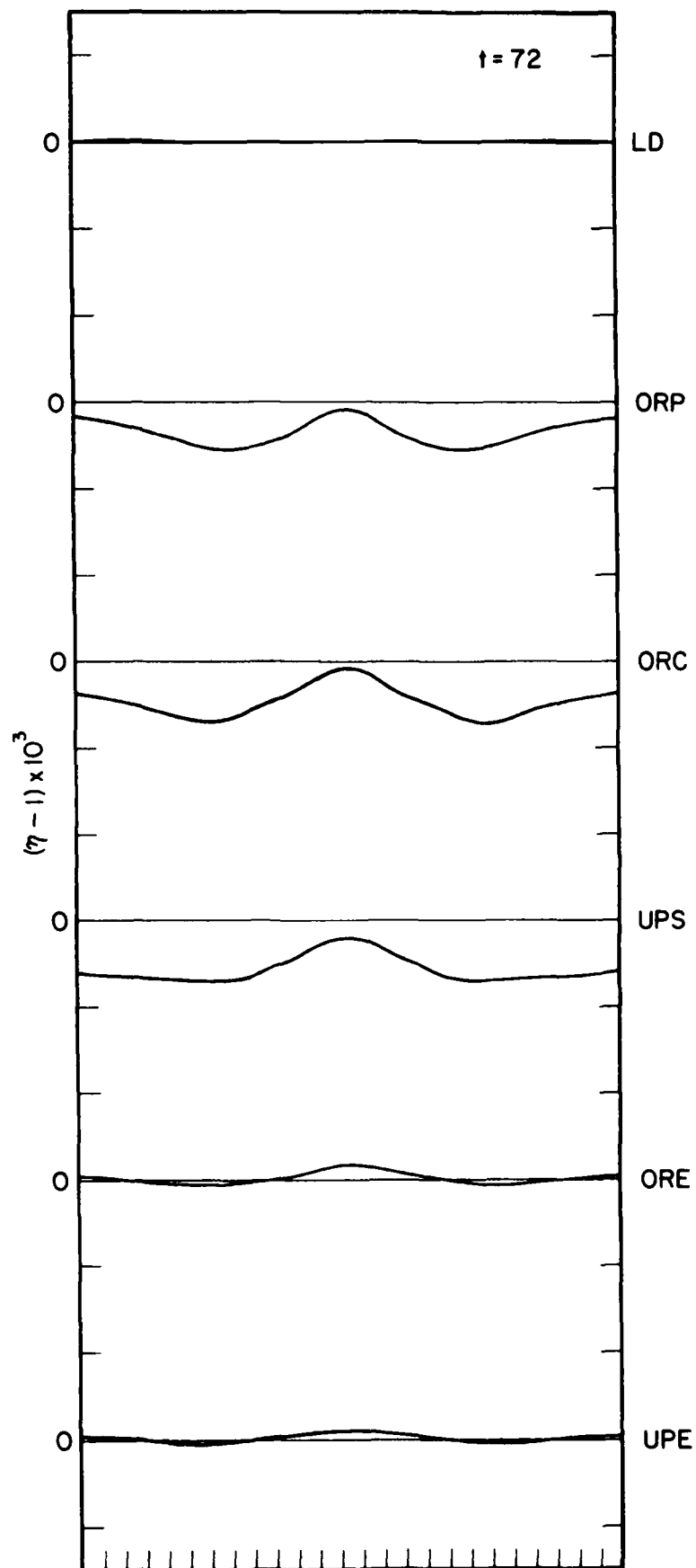


Figure 9. As fig. 5.

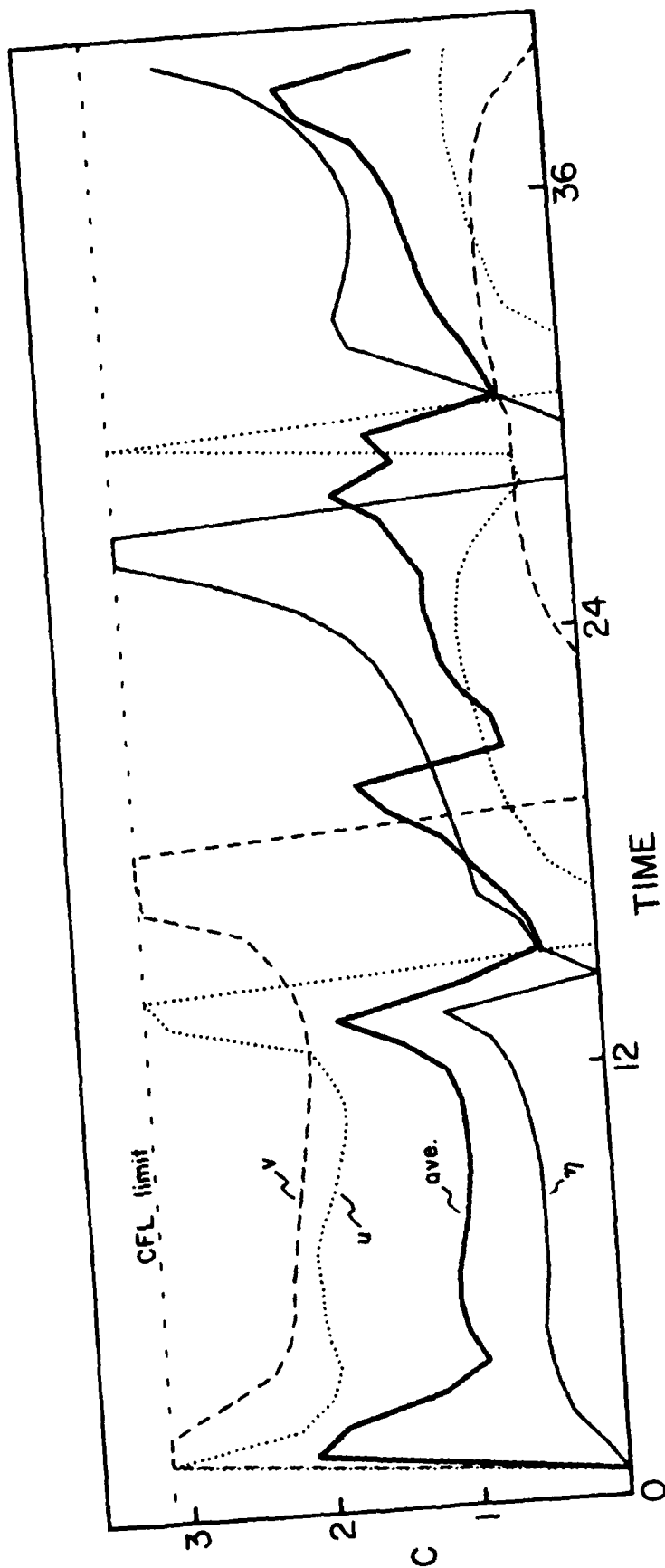


Figure 10. Phasespeed calculated in ORP for  $\eta$ ,  $u$ , and  $v$  as a function of time. Average phasespeed calculated in ORPA (labeled "ave").

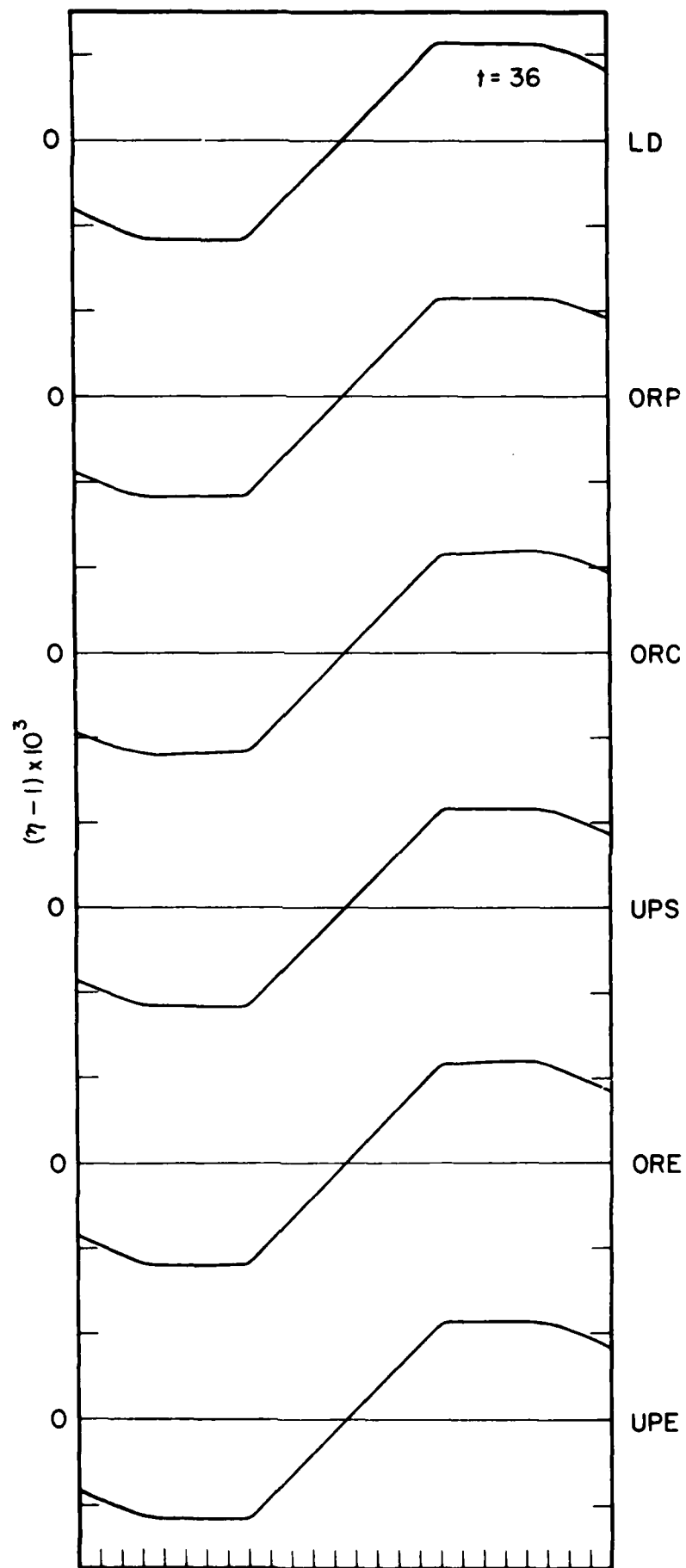


Figure 11. As fig. 6.

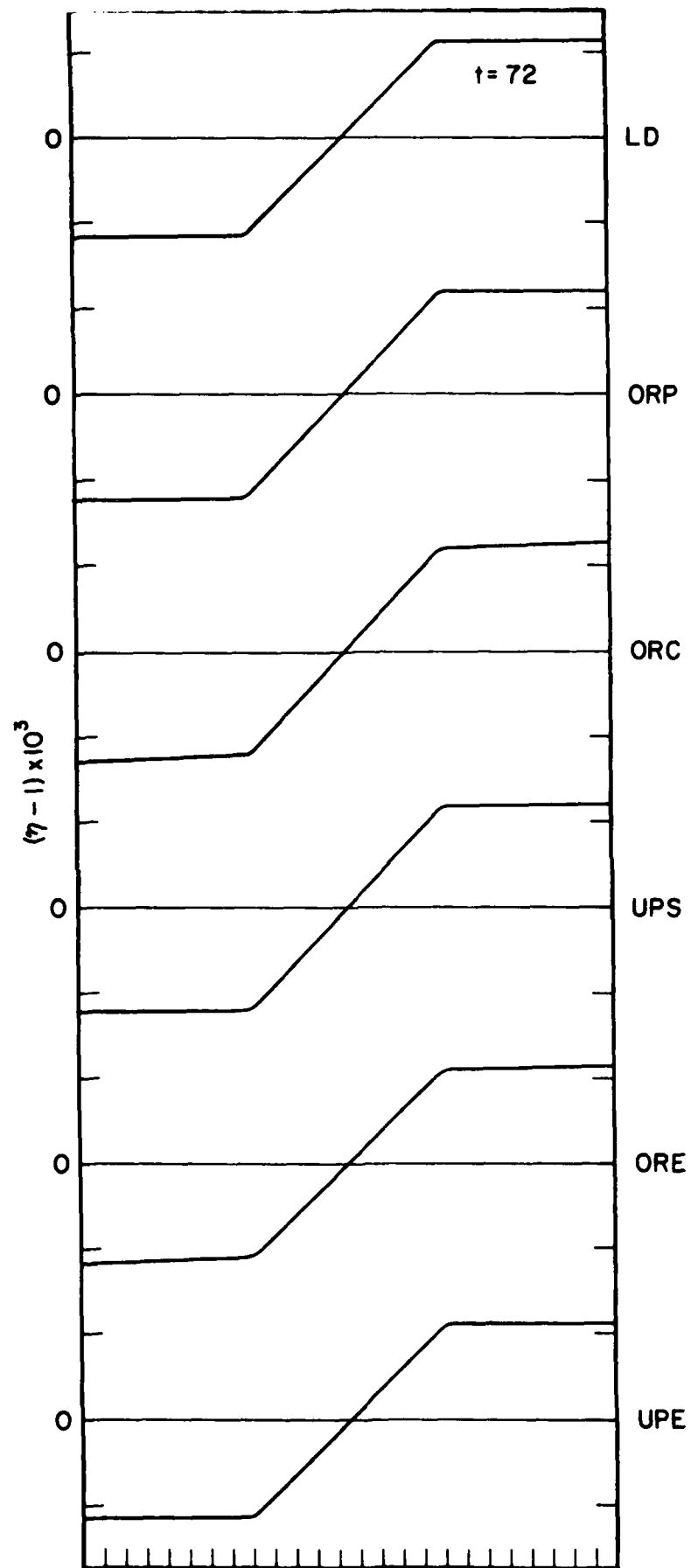


Figure 12. As fig. 7.



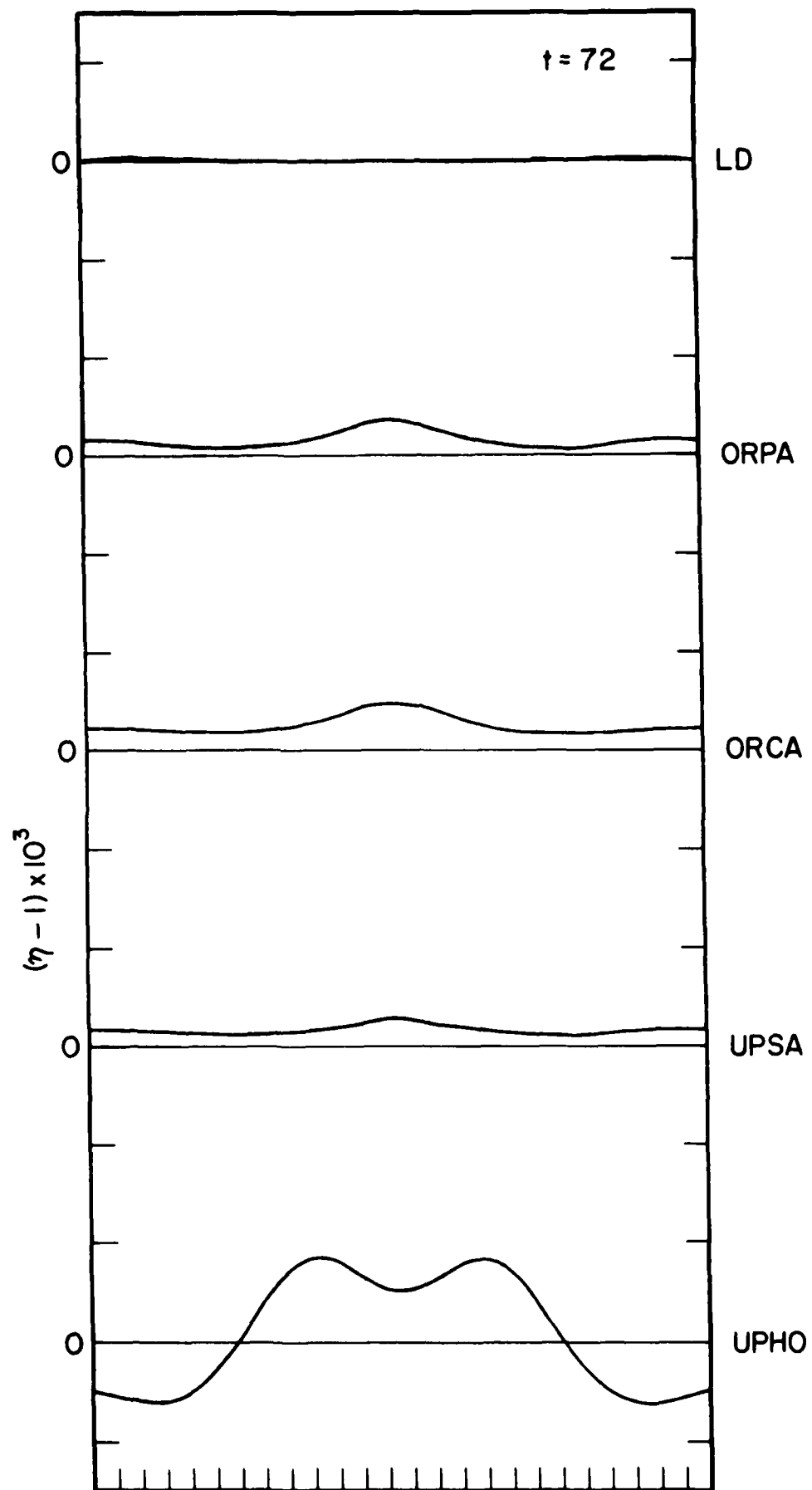


Figure 13. As fig. 5.

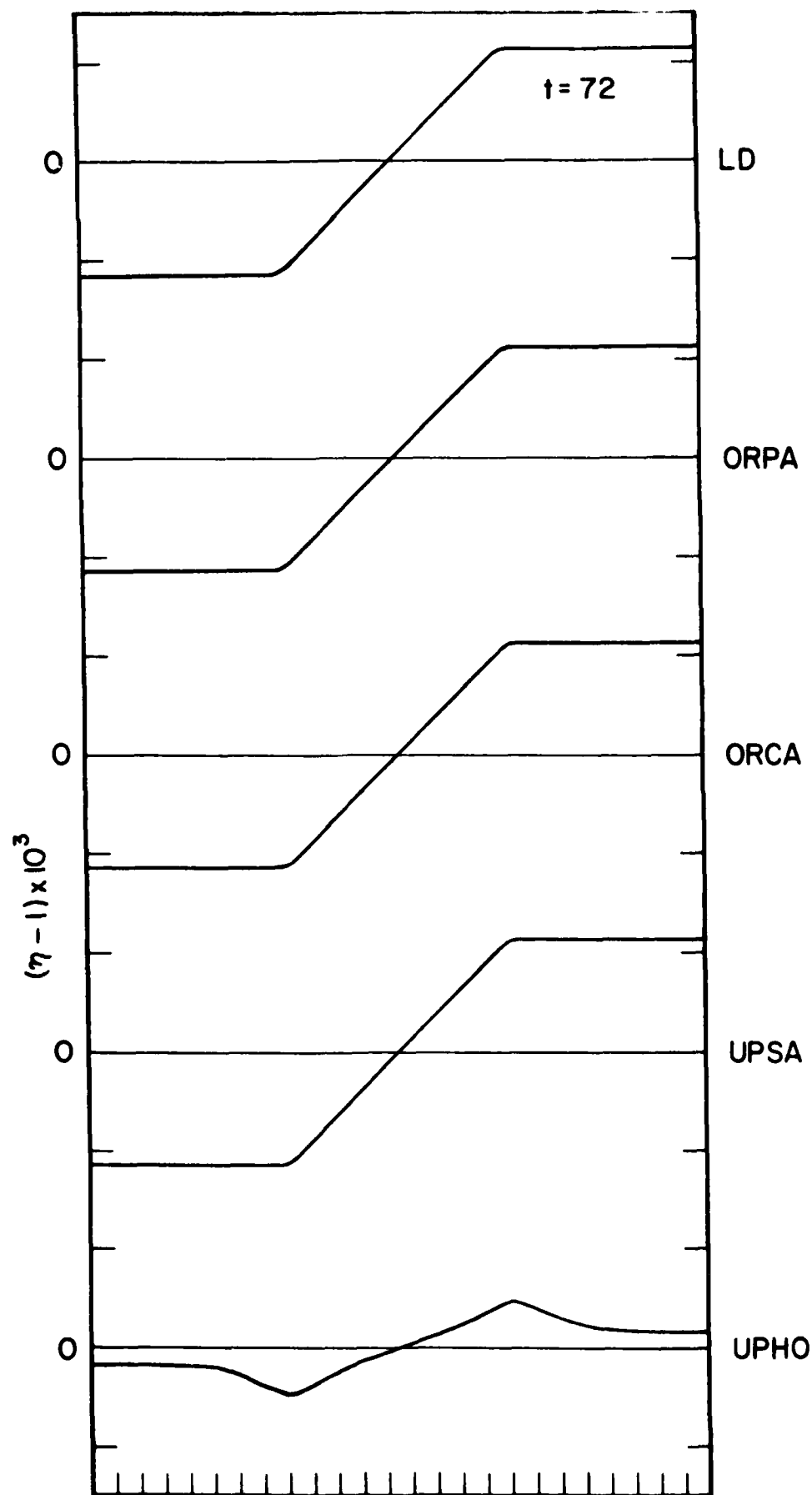


Figure 14. As fig. 7.

DTIC

FILMED

4-86

END